polymers

MDPI

Article

Antibacterial Capability, Physicochemical Properties, and Biocompatibility of $nTiO_2$ Incorporated Polymeric Scaffolds

Cijun Shuai [1,2,3], Chenying Shuai [2], Pei Feng [2], Chengde Gao [2], Shuping Peng [4,*] and Youwen Yang [1,2,*]

1 Jiangxi University of Science and Technology, Ganzhou 341000, China; shuai@csu.edu.cn
2 State Key Laboratory of High Performance Complex Manufacturing, College of Mechanical and Electrical Engineering, Central South University, Changsha 410083, China; shuaichenying@csu.edu.cn (C.S.); fengpei@csu.edu.cn (P.F.); gaochengde@csu.edu.cn (C.G.)
3 Key Laboratory of Organ Injury, Aging and Regenerative Medicine of Hunan Province, Changsha 410008, China
4 The Key Laboratory of Carcinogenesis of the Chinese Ministry of Health, Xiangya Hospital, Cancer Research Institute, Central South University, Changsha 410008, China
* Correspondence: shuping@csu.edu.cn (S.P.); yangyouwen@csu.edu.cn (Y.Y.); Tel.: +86-731-84805412 (S.P.); Fax: +86-731-88879044 (S.P.)

Received: 29 January 2018; Accepted: 13 March 2018; Published: 16 March 2018

Abstract: Postoperative infection is a common risk which brings about failure in bone transplantation. In this study, nano titanium dioxide ($nTiO_2$) was incorporated into Polyetheretherketone/polyglycolicacid (PEEK/PGA) blends to construct antibacterial scaffolds via selective laser sintering. Antibacterial capability was assessed using *Escherichia coli* (*E. coli*) and *Staphylococcus aureus* (*S. aureus*). The results demonstrated that the scaffolds with $nTiO_2$ presented an effective antibacterial activity, which might be attributed to that $nTiO_2$ would do the mechanical and oxidative damage to bacteria by occurring contact actions and generating reactive oxygen species (ROS), and thus killed bacteria from structure and function. Moreover, $nTiO_2$ could enhance the tensile strength and modulus of scaffolds due to the reinforcing effect and its uniform disperse. And the cell culture experiments showed that $nTiO_2$ stimulated cellular attachment and proliferation. Besides, it also elevated the hydrophily and thermal stability of scaffolds. These results suggested that the polymeric scaffolds incorporated $nTiO_2$ had potential application in bone tissue engineering.

Keywords: nano titanium dioxide; antibacterial capability; cellular attachment; polymeric scaffolds

1. Introduction

There exists a risk of bacterial infections after artificial bone transplantation [1,2]. It is a common method to use antibiotics for preventing bacterial infections [3,4]. However, their long-term application would bring about toxic and adverse effects including hypersensitivity, immune suppression, and allergic reaction [5–7]. In addition, the abuse of antibiotics would cause drug resistance in bacteria [8]. Therefore, it is necessary to develop antibacterial scaffolds to deal with the implant-associated bacterial infections. A potential strategy is to incorporate antibacterial materials into scaffolds [9–12].

Acknowledged as a typical inorganic antibacterial biomaterial, nano titanium dioxide ($nTiO_2$) has been given much attention due to its strong and broad-spectrum antimicrobial action [13–16]. Moreover, $nTiO_2$ presents good biocompatibility, excellent biosecurity, and extraordinary hydrophilicity [17–19]. Besides, it is a desired candidate as a reinforcing filler in a polymeric matrix [20]. Further, the strength of bone-titanium integrations is considerably greater compared with other nanoparticles [21]. Polyetheretherketone/polyglycolicacid (PEEK/PGA) blends have potentially used in bone repair

because of their remarkable processability, biocompatibility, and degradation property [22]. As an additive manufacturing method, selected laser sintering (SLS) is able to construct scaffolds with complex shapes and accurate interconnected porous structures [23–25].

Recently, Wu et al. fabricated TiO_2/Poly(lactic-co-glycolic acid) composite biomaterial by a sol–gel method and confirmed that the composites possessed biocompatibility and antibacterial properties [26]. González-García et al. prepared Polyurethanes/TiO_2 hybrid via a sol–gel reaction and found that the hybrids exhibited improved thermal and mechanical properties compared with the polyurethanes matrix [27]. Roether et al. developed Poly(glycerol sebacate)/Poly(3-hydroxybutyrate)-TiO_2 nanocomposite through solvent casting and discovered that adding TiO_2 into the scaffolds led to an encouraging improvement in mechanical properties and wettability [28]. However, scarce works focused on the comprehensive performances of $nTiO_2$ contained scaffolds fabricated by selective laser sintering.

In this study, $nTiO_2$ was incorporated into PEEK/PGA blends. The scaffolds with $nTiO_2$ were prepared via selective laser sintering. The effect of $nTiO_2$ on antibacterial activity against *Escherichia coli* (*E. coli*) and *Staphylococcus aureus* (*S. aureus*) was evaluated. And the microstructures and thermal properties of the scaffolds were characterized. Meanwhile, their mechanical properties, degradation behavior, and cell response were also investigated.

2. Materials and Methods

2.1. Materials and Scaffolds Preparation

PEEK (powder size 20–50 μm, Mw: 270,000 g/mol, Purity ≥99.5%) was supplied by Dongguan Guanhui Plastic Materials Co., Ltd. (Dongguan, China). PGA (powder size ~40 μm, Mw: 1,000,000 g/mol, Purity ≥99.5%) was purchased from Shenzhen Polymtek Biomaterial Co., Ltd. (Shenzhen, China). $nTiO_2$ (rutile) (powder size ~30 nm, Purity ≥99.9%) was obtained from Nanjing Emperor Nano Material Co., Ltd. (Nanjing, China). And all the other agents were analytical reagents.

The overall preparation procedure of the scaffolds was represented in Figure 1. Firstly, TiO_2 nanoparticles and PEEK/PGA blended powders (8:2 mass ratios) were dissolved in alcohol and dispersed by bath ultrasonication over 20 min, respectively. Subsequently, $nTiO_2$ solution was added into PEEK/PGA solution, and then they were homogenized via ultrasonic cleaner for 30 min. To further improve the dispersion of $nTiO_2$, the mixed solution was grinded using a variable frequency planet-type grinding mill for 60 min. After that, the obtained solution was filtered through qualitative filter paper and was exsiccated at 50 °C for 24 h in a drying cabinet. Finally, a series of PEEK/PGA-$nTiO_2$ mixed powders were obtained for scaffold preparation, with $nTiO_2$ contents of 0, 1, 3, 5, and 7 wt %, respectively.

The scaffolds with $nTiO_2$ loading of 0 wt % (PEEK/PGA), 1 wt % (PEEK/PGA-1%$nTiO_2$), 3 wt % (PEEK/PGA-3%$nTiO_2$), 5 wt % (PEEK/PGA-5%$nTiO_2$), and 7 wt % (PEEK/PGA-7%$nTiO_2$) were fabricated via selective laser sintering. The system consisted of a CO_2 laser, scanner system, sintering platform and corresponding control system. During sintering, the laser beam selectively scanned the powders according to the cross-sectional area of scaffolds. The sintering platform was subsequently moved down a layer thickness, and the sintering procedure was repeated. The interconnected porous scaffold with an overall size of 13 mm × 10 mm (diameter × height) was manufactured, as presented in Figure 1.

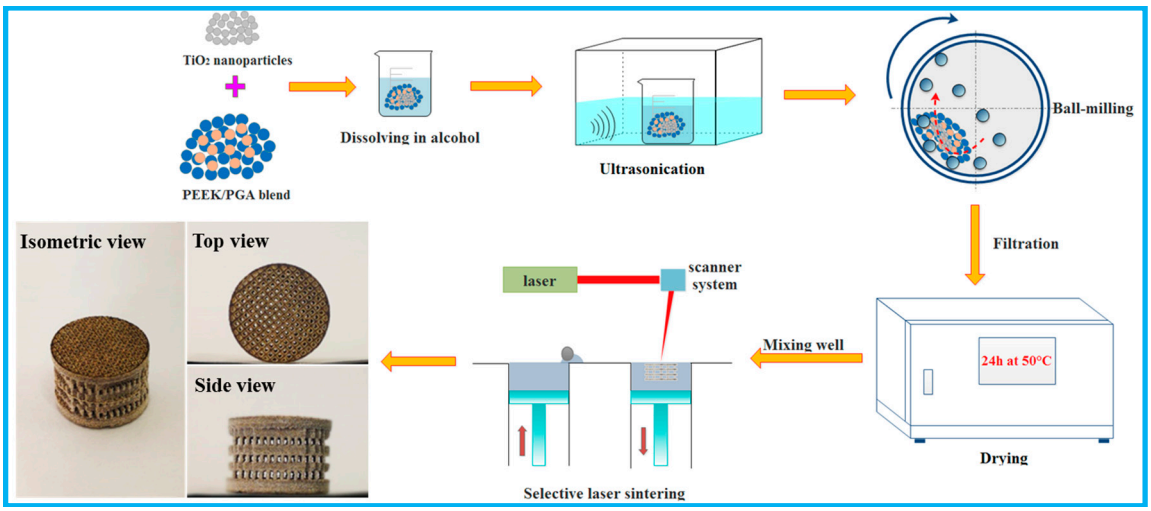

Figure 1. Schematic of the scaffold preparation process.

2.2. Characterization

The phase constituents of the scaffolds were determined using an X-ray diffractometer (XRD, Rigaku Co., Tokyo, Japan). The XRD data were recorded at the scanning rate of 8°/min in 2θ range from 10° to 80°. Fourier transform infrared spectroscopy (FTIR) analysis was performed with Nicolet 6700 spectrometer (Thermo Scientific Co., Madison, WI, USA) in the wavenumber range from 4000 cm^{-1} to 600 cm^{-1}. Moreover, the scaffolds were analyzed through a scanning electron microscopy (SEM; JEOL JSM 7600F, Tokyo, Japan). All the specimens were sputtered by platinum (JFC-1600, Jeol Co., Tokyo, Japan). And the elemental constituents were investigated by an energy dispersive spectroscopy (EDS).

Tensile strength of the scaffolds was tested with an electronic universal testing machine at a crosshead speed of 0.5 mm/min (WD-D1, Shanghai Zhuoji Instruments Co., Ltd., Shanghai, China). The scaffold samples ($10 \times 10 \times 5$ mm^3) were tested at ambient temperature and five samples for each group were tested. Then the mean value was calculated. Besides, the tensile modulus was obtained through the initial slope of the stress-strain curve.

The thermal stability of the scaffolds was investigated by thermogravimetric analysis (TGA) with STA-200 Instruments (Optoma Europe Ltd., Hertfordshire, UK). Specimens (approximately 15 mg) were sealed in aluminum pan. Then temperature was scanned from 25 °C to 700 °C at a heating rate of 10 °C/min under an inert atmosphere. Dynamic differential scanning calorimetry (DSC) experiments were conducted under a nitrogen atmosphere. Samples (approximately 10 mg) were heated from 25 °C to 700 °C. The steps were implied at a constant rate of 10 °C/min, and transition temperatures were regarded as the peak minimum of calorimetric curve.

Water contact angle of scaffolds was measured to evaluate the wetting property using a KSV CAM 200 optical contact angle meter (KSV Instruments Ltd., Helsinki, Finland). Deionized water drops, which were used as probe liquid, were place on the samples surface at room condition. Also, five independent measurements for each group were averaged to calculate contact angle.

2.3. Antibacterial Activity Assay

The antibacterial capability of scaffolds was assessed by plate count method against *E. coli* (ATCC, 25922) and *S. aureus* (ATCC, 12600). Prior to the experiments, all the scaffolds were sterilized in a steam autoclave and desiccated on superclean bench. The 10 µL solution with *E. coli* and 10 µL solution with *S. aureus* at a density of 1×10^7 CFU/mL was added into each scaffold, followed by using sterilized polyethylene films to cover their surface. After anaerobic cultivation for 24 h at 37 °C, the bacteria on scaffolds were collected to new agar plates, and then the number of viable bacteria was counted using plate count method. The antibacterial rate was estimated following the equation:

$A\% = [(B - E)/B] \times 100\%$, where $A\%$ was the antibacterial rate, E and B were the bacterial number of the experimental groups and blank control group, respectively. Additionally, the scaffolds without TiO_2 were used as blank control. Five tests were conducted to obtain the average value.

2.4. Cell Culture

Human osteoblast-like cells (MG-63) were used to investigate the compatibility of the scaffolds. The cell lines were maintained and cultured in the Dulbecco's modified Eagle's medium supplemented with 10% FBS and 1% penicillin/streptomycin. The scaffolds were placed in a 12-well plate after being sterilized in the autoclave. After that, the scaffolds seeded with 2×10^4 cell/cm^2 of cells were cultivated in a humid incubator with 5% CO_2 atmosphere at 37 °C, and culture medium was refreshed every other day. After predetermined incubation time, the scaffolds were fetched out, fixed in 4% glutaraldehyde for 1 h, and then dehydrated using gradient ethanol. In the end, cell attachment and spread were investigated under SEM after they were entirely dried.

At 1, 3, and 5 days of incubation, the scaffolds were rinsed with phosphate buffer solution (PBS) twice after being removed out, and then adherent cells were immobilized with paraformaldehyde, permeabilized with 0.5% Tween 20. Afterwards, the cells were purged again and incubated into PBS including 4 μM EthD-1 and 2 μM calcein AM for 25 min. In the end, the cells were observed under a fluorescence microscope.

In addition, microculture tetrazolium test (MTT) assay was performed to estimate the cell proliferation. After being fostered for 1, 3, and 5 days, 20 μL of MTT solution was dropped into cell culture plates. Subsequently, it was kept at 37 °C for 3 h, and formazan crystals were completely dissolved with 200 mL dimethyl sulphoxide (DMSO) after throwing off the supernatants. Finally, the absorbency was measured with a microplate reader at 570 nm. Five parallel experiments for each group were numerated. Moreover, the culture medium was used as blank group.

2.5. In Vitro Degradation Study

The in-vitro degradation behavior of the scaffolds was evaluated using PBS solution (pH = 7.4). All the specimens were first weighed (M_i). Whereafter, they were immersed in the solution and incubated at 37 °C for prearranged periods (7, 14, 21, and 24 days). The PBS was renewed every 3 days. At each prescribed time, the specimens were withdrawn and mildly rinsed with deionised water, and then entirely dried at 40 °C to obtain final weight (M_f). The weight loss (W_l) were determined using following formula:

$$W_l = (M_i - M_f)/M_i \quad (1)$$

2.6. Statistical Analysis

All experimental data were listed as the mean ± standard deviation (SD). One way ANOVA was implemented to determine statistical significance. In all analyses, $p < 0.05$ was considered to be statistically significant.

3. Results and Discussion

3.1. Microstructural Characteristics

The XRD pattern of PEEK/PGA-nTiO_2 scaffolds loading different nTiO_2 concentration was shown in Figure 2A. PEEK phase and PGA phase, as the predominant components of the scaffolds, were distinctly displayed in all patterns. XRD diffraction peaks around 2θ of 27.42°, 36.10° and 54.2° could be indexed to the characteristic peaks (101), (004), and (200) of rutile TiO_2. Meanwhile, with the increase of nTiO_2, these peaks increased in intensity. In addition, no extra peaks of other phase were visible. In fact, a rise in crystallinity was found for scaffolds with low nTiO_2 contents, whereas the reverse trend was observed at high nTiO_2 contents. The results hinted a change from promotion to retardation in the crystallization rate of the polymer with increasing nanoparticle concentration.

Thus, the nucleating effect of the nanoparticles likely led to higher degree of crystallinity at low $nTiO_2$ concentration, whereas the increased $nTiO_2$-matrix interactions could prevail over the nucleation effect at higher nanofiller concentration. An analogous phenomenon has been reported for PEEK composites reinforced with inorganic WS_2 nanoparticles, where the nucleation of the polymer crystals was favored at low nanofiller contents [29].

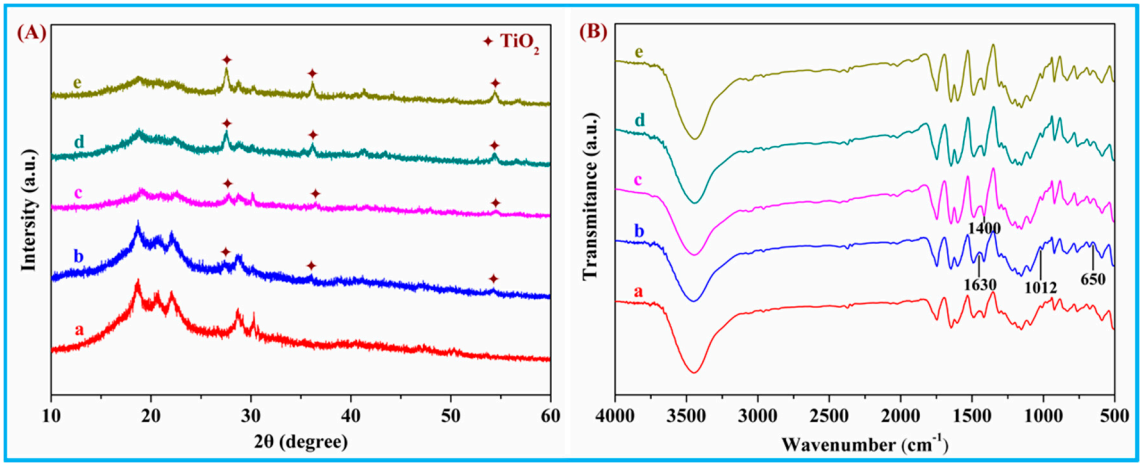

Figure 2. (**A**) X-ray diffractometer (XRD) spectra and (**B**) Fourier transform infrared spectroscopy (FTIR) spectra for the scaffolds with (a) 0 wt %; (b) 1 wt %; (c) 3 wt %; (d) 5 wt %; and (e) 7 wt % $nTiO_2$.

FTIR spectra of PEEK/PGA-$nTiO_2$ scaffolds were recorded (Figure 2B). The spectrum of $nTiO_2$ displayed peaks at 1630 and 1012 cm^{-1} arising from the bending vibration of coordinated H_2O and Ti-OH. The peak at ~650 cm^{-1} was related to the Ti-O-Ti stretching motion, and that at ~1400 cm^{-1} corresponded to $nTiO_2$ lattice vibrations. The results demonstrated that there was a successful combination of $nTiO_2$ in the scaffolds.

The sintered surface of the scaffolds was characterized by SEM, and the composition of the PEEK/PGA and PEEK/PGA-5%$nTiO_2$ scaffolds was detected by EDS with orange square area (Figure 3). The morphology of PEEK/PGA scaffolds appeared glossy and flat. After the incorporation of $nTiO_2$, some particles arose in matrix. Moreover, the particles dispersed uniformly in the polymeric matrix when filler concentration was no more than 5 wt %, and they were evaluated using EDS (Figure 3g). The emergence peaks of Ti proved that these particles were $nTiO_2$. Nevertheless, the $nTiO_2$ formed agglomeration when further increasing its concentration (Figure 3e). The results might be due to that excessive $nTiO_2$ could reduce the distance between nanoparticles, and thus increased their interaction force and the chance of contacts [30,31].

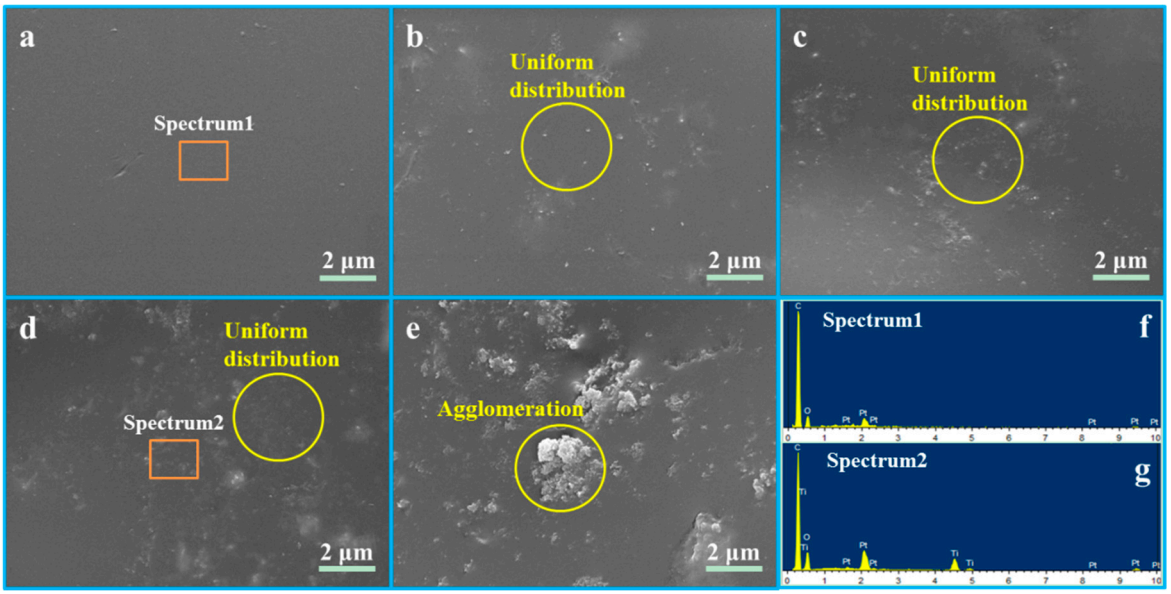

Figure 3. Morphology of (**a**) PEEK/PGA scaffold, (**b**) PEEK/PGA-1%nTiO_2 scaffold, (**c**) PEEK/PGA-3%nTiO_2 scaffold, (**d**) PEEK/PGA-5%nTiO_2 scaffold, (**e**) PEEK/PGA-7%nTiO_2 scaffold, and (**f**), (**g**) energy dispersive spectroscopy (EDS) spectra of the marked region.

3.2. Thermal Stability and Hydrophilicity

DSC was utilized to assess the effects of nTiO_2 on melting behavior of scaffolds, with results depicted in Figure 4a. DSC curves of PEEK/PGA scaffolds exhibited two apparent endothermic peaks at approximately 218 °C and 337 °C, which accorded with endothermic peaks of PGA and PEEK [32,33]. Moreover, the melt temperatures of scaffolds were increased with increasing nTiO_2 compared with those of the scaffolds without nTiO_2. The results were mainly because of the nucleation effect of TiO_2 nanoparticles, since they could hasten the development of nucleus [34].

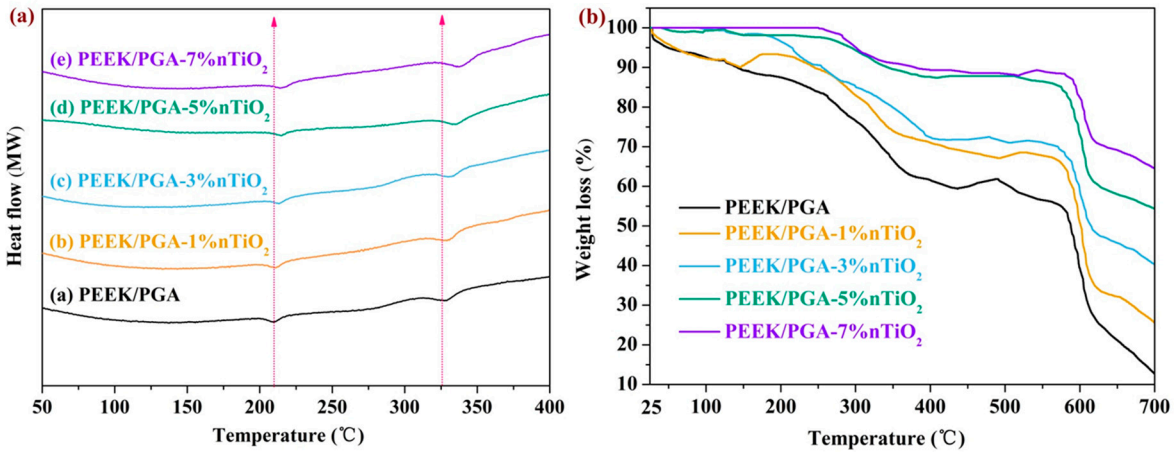

Figure 4. (**a**) Differential scanning calorimetry (DSC) curve and (**b**) thermogravimetric analysis (TGA) curve of the scaffolds with different nTiO_2 contents.

Thermal characterization of the scaffolds was investigated using TGA analysis (Figure 4b). It appeared that the scaffolds with nTiO_2 and the scaffolds without nTiO_2 decomposed by a two-step process, and the TGA profile of the scaffolds with nTiO_2 scaffolds shifted to high temperature compared with that of the scaffolds without nTiO_2. Moreover, the scaffolds with nTiO_2 showed less weight loss than the scaffolds without nTiO_2. The results suggested that the scaffolds with nTiO_2 could

elevate thermal stability. It was believed that $nTiO_2$ could act as a barrier against the transportation of decomposed product [35]. On the other hand, $nTiO_2$ possessed a high thermal conductivity, which made contributions to the heat dissipations within the polymeric matrix [36].

The hydrophilicity of scaffolds is well-known as a crucial factor to determine cell response, which could be assessed by water contact angle (Figure 5). It could be visible that the contact angle reduced with increasing $nTiO_2$, hinting that $nTiO_2$ would improve the hydrophilicity of scaffolds. The cause might be that $nTiO_2$ was hydrophilic owing to the existence of unsaturated reactive hydroxyl groups (-OH) [37].

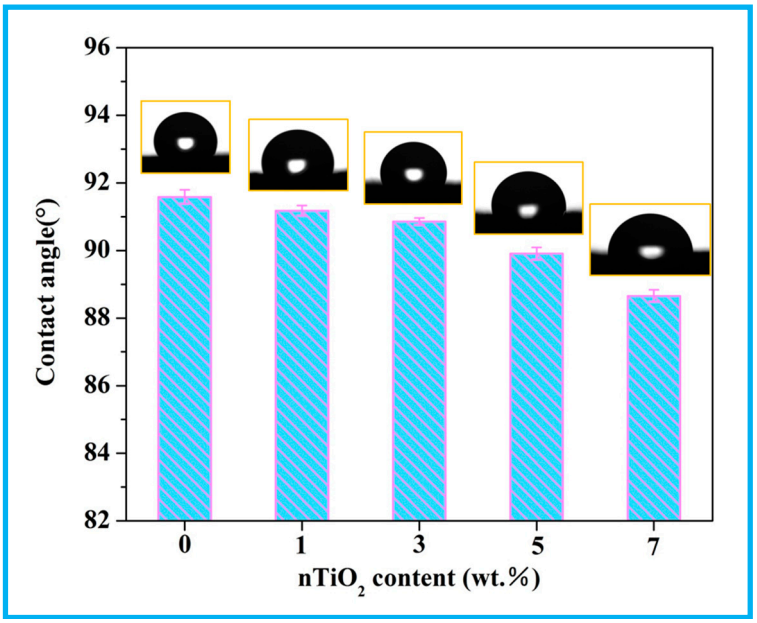

Figure 5. Water contact angle of the scaffolds with different $nTiO_2$ contents.

3.3. Antibacterial Activity

The antibacterial capability of the scaffolds was explored against *E. coli* and *S. aureus* (Figure 6). As could be observed, the scaffolds without $nTiO_2$ did not exhibit antimicrobial activity. While the scaffolds with $nTiO_2$ presented antibacterial activity, and their antibacterial activity rose upon increasing $nTiO_2$, displaying a maximum at 5 wt % $nTiO_2$, and then declined. The results implied that $nTiO_2$ played a vital role in antibacterial capability and could be explained that the overall interaction between nanofiller and bacteria would be weak at low $nTiO_2$ contents [38]. While at high contents nanoparticle clusters reduced the effective surface-to-volume ratio of nanofiller, thus the overall interaction between $nTiO_2$ and bacteria was also decreased [39].

The possible antibacterial mechanisms were that (Figure 7): $nTiO_2$ could react with water and oxygen, thus generating active oxygen species (ROS). ROS would make bacteria produce oxidative stress when its concentrations exceed the scavenging activity of bacterial antioxidant defense system, subsequently damaging the structure and function of the bacteria [40]. Besides, the contact action between $nTiO_2$ and bacterial cell wall would generate mechanical stress, leading to the deformation of bacterial cell membrane [41]. Then $nTiO_2$ would be absorbed into the bacteria and damage them from the interior.

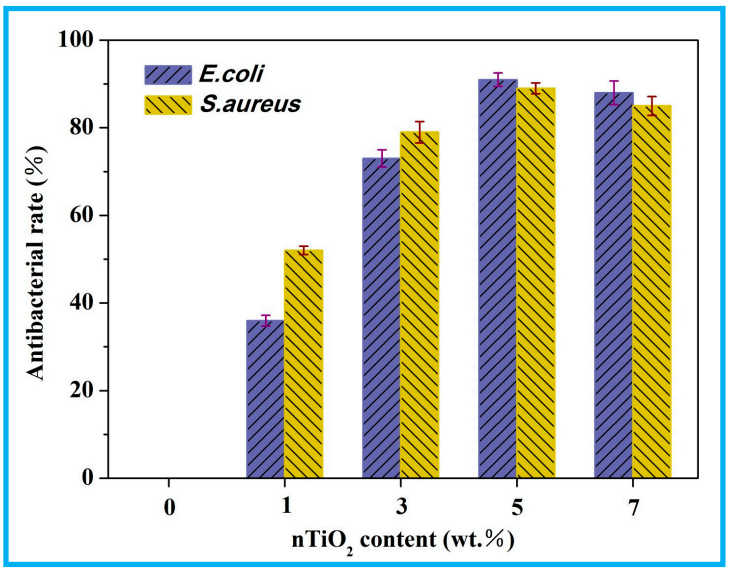

Figure 6. Antibacterial rate of the scaffolds with different $nTiO_2$ contents.

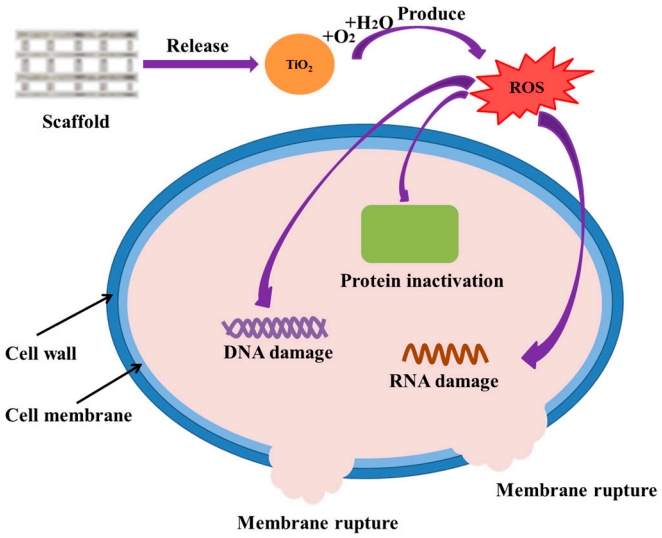

Figure 7. Possible antibacterial mechanisms of PEEK/PGA-$nTiO_2$ scaffolds.

3.4. Mechanical Properties

The mechanical properties of PEEK/PGA-$nTiO_2$ scaffolds were examined (Figure 8). Their tensile strength and modulus kept increasing when $nTiO_2$ content was until 5 wt %. The incorporation of 5 wt % $nTiO_2$ enhanced tensile strength to 51.20 MPa, being 35% higher than that of PEEK/PGA scaffolds. At the same time, tensile modulus increased to 3.87 GPa, which was 48% higher than that of polymeric scaffold. The improvements were owing to the reinforcement effect and uniformly-dispersed $nTiO_2$. Noted that tensile strength and modulus would increase with inorganic filler contents were common in polymeric matrix [42–44]. However, when $nTiO_2$ were excessive, the variation tendency of mechanical properties started to reverse. It could be explained that $nTiO_2$ occurred agglomeration with its increase and leading to inhomogeneous dispersion. The results of the antibacterial experiments and mechanical experiments indicated that the optimal $nTiO_2$ content was 5 wt % in this study. Therefore, the comprehensive performances of the scaffolds with 5 wt % $nTiO_2$ were evaluated in follow-up experiments.

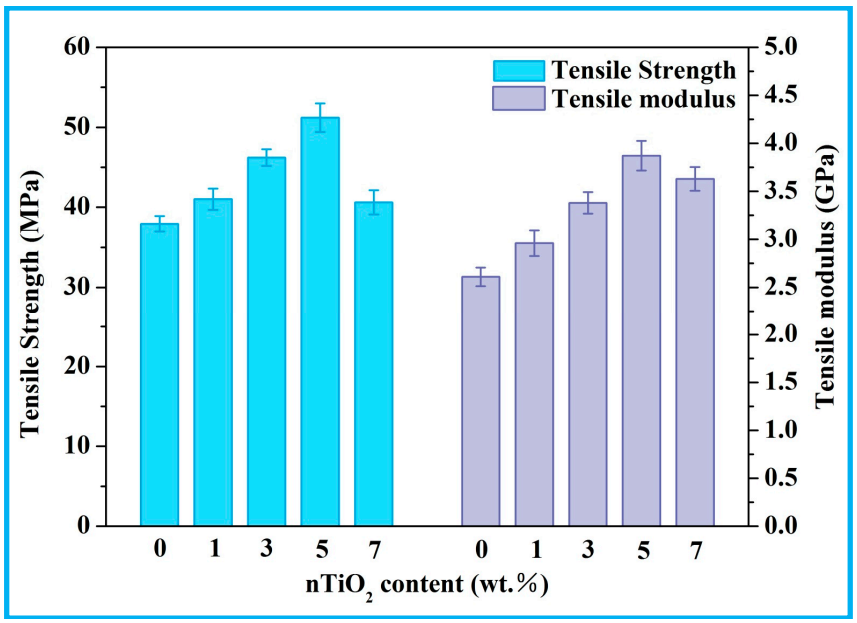

Figure 8. Tensile strength and modulus of the scaffolds with different $nTiO_2$ contents.

3.5. In Vitro Degradation

The pH of scaffolds during in-vitro degradation was depicted in Figure 9. It decreased from 7.4 on account of the released acidic degradation product of PGA. In the meantime, it was evident that pH of the scaffolds with $nTiO_2$ dropped slowly compared with that of the scaffolds without $nTiO_2$. This was because the degradation of PGA was composed of a hydrolysis process, which would increase acid atmosphere, and hence its pH would present a downward trend. While the incorporation of $nTiO_2$ provided a buffering effect that the scaffolds with $nTiO_2$ could absorb water and then formed titanium hydroxide (Ti-OH groups) [45], consequently prevented the drop in pH.

In-vitro degradation was evaluated by weight loss. As the immersion time prolonged, weight loss of the scaffolds gradually increased. After degrading for 28 days, weight loss of the scaffolds with $nTiO_2$ present a bit lower than that of the scaffold without $nTiO_2$ (8.64% and 9.72%, respectively). It might be ascribed to that titanium hydroxide (Ti-OH groups) formed on the surface of $nTiO_2$ would neutralize the acid degradation products of PGA [46], leading to the decrease of PGA degradation.

3.6. Biocompatibility Studies

The adhesion morphologies of MG-63 cells cultivated on the scaffolds were showed (Figure 10). The scaffolds with $nTiO_2$ showed a better cell adhesion than that of the scaffolds without $nTiO_2$ after cultured for one day. After 3 days of incubation, cells on the scaffolds with $nTiO_2$ presented affluent filopodias and were spread extensively on the scaffolds. While the scaffolds without $nTiO_2$ had few filopodias. When cultured for 5 days, the cells secreted extracellular matrix (ECM) and formed confluent cells layer on the both of scaffolds. Besides, almost entire region of the scaffolds with $nTiO_2$ were covered with the cells and formed a thicker cell layer than that on the scaffolds without $nTiO_2$.

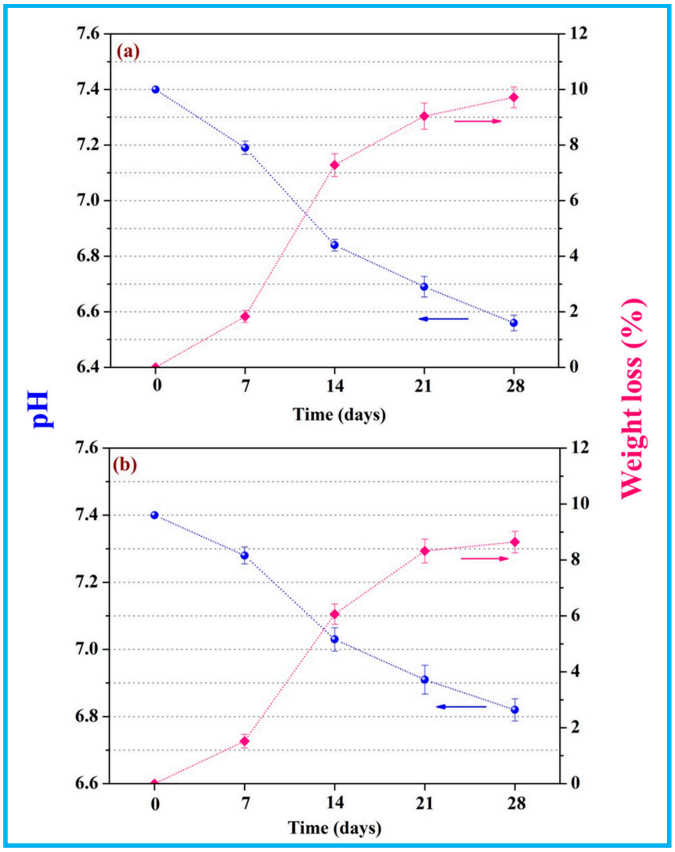

Figure 9. pH value and weight loss of (**a**) PEEK/PGA scaffolds and (**b**) PEEK/PGA-5%nTiO_2.

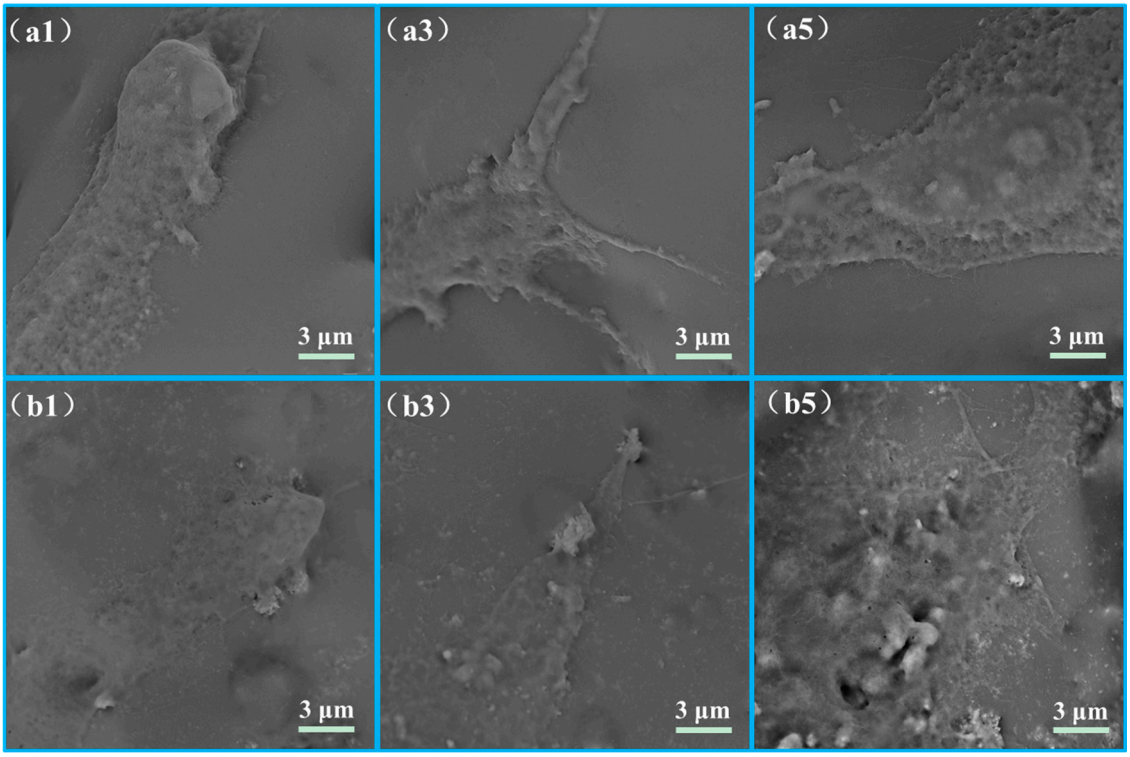

Figure 10. Cells on the (**a1**–**a5**) PEEK/PGA and (**b1**–**b5**) PEEK/PGA-5%nTiO_2 scaffolds after culture for 1, 3, and 5 days.

In order to further illustrate the attachment and proliferation of the MG-63 cells, the cell fluorescence experiment was carried out (Figure 11). The cells on the scaffolds exhibited light green and related cytoblast presented purplish blue. It was apparent that cell number increased with the increase of incubation time. More importantly, the change trend of the cells cultured on the scaffolds with $nTiO_2$ was more obvious than the cells cultured on the scaffolds without $nTiO_2$. The results indicated that $nTiO_2$ was conducive to cellular attachment and spread.

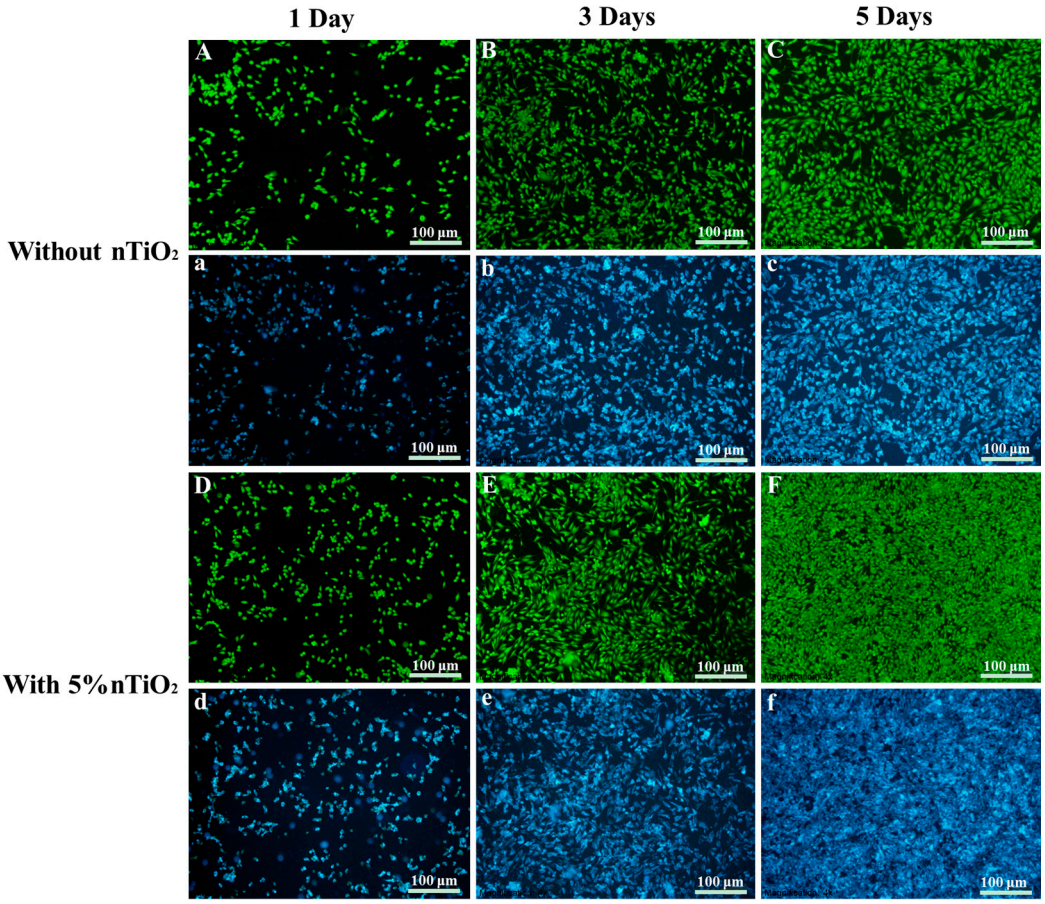

Figure 11. Fluorescence microscopy images (live cells appeared as bright green dots and related cytoblast as purplish blue dots) of MG-63 cells on (**A**–**C** and **a**–**c**) PEEK/PGA and (**D**–**F** and **d**–**f**) PEEK/PGA-5%$nTiO_2$ scaffolds after culture for 1, 3, and 5 days.

The cell proliferation on the PEEK/PGA-5%$nTiO_2$ was evaluated using MTT assay (Figure 12). Compared with the blank group, it was obvious that both of the scaffolds demonstrated high absorbance values during the whole culture time, which indicated an enhanced cell proliferation. Moreover, it should be noted that the cell density on the scaffolds with $nTiO_2$ was higher than that on the scaffolds without $nTiO_2$. The results implied that $nTiO_2$ could promote the proliferation of MG63 cells. It could be concluded that $nTiO_2$ was in favour of cellular proliferation and attachment, which might be due to the favourable biocompatility of $nTiO_2$ [47]. Further, the scaffolds with $nTiO_2$ were more hydrophilic, which could promote the interaction between cells and scaffolds [48,49].

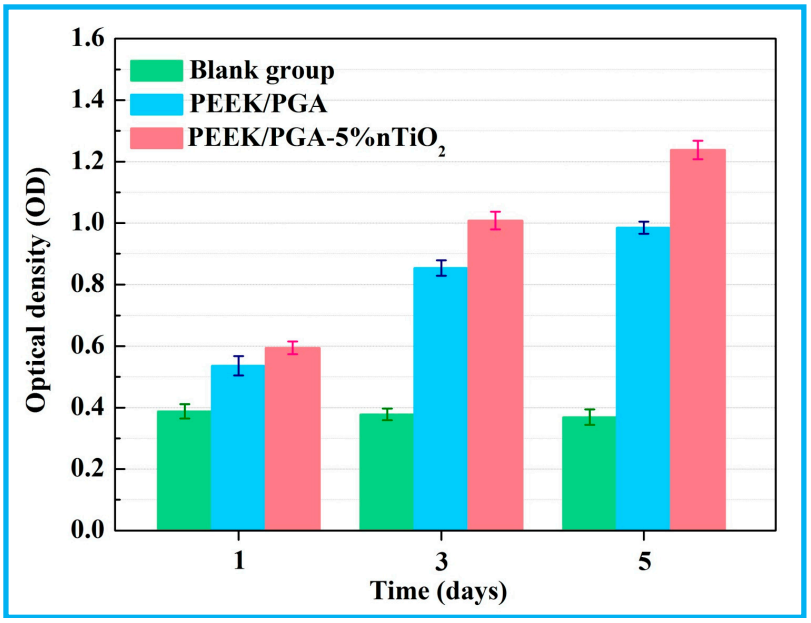

Figure 12. Proliferation of MG-63 cells on PEEK/PGA-5%$nTiO_2$ and PEEK/PGA scaffolds after culture for 1, 3, and 5 days.

4. Conclusions

PEEK/PGA-$nTiO_2$ scaffolds were fabricated via SLS. The polymeric scaffolds with $nTiO_2$ possessed significant antibacterial capability. Moreover, their tensile strength and modulus were improved by 35% and 48% with 5 wt % $nTiO_2$, respectively. And the hydrophily and thermal stability of the scaffolds were also elevated. Furthermore, MG-63 cell experiments testified that $nTiO_2$ could promote cellular attachment and proliferation. Hence, PEEK/PGA scaffolds with $nTiO_2$ might be promising implants for tissue engineering.

Acknowledgments: This work was supported by the following projects and funds: (1) The Natural Science Foundation of China (51575537, 81572577, 51705540); (2) Overseas, Hong Kong, and Macao Scholars Collaborated Researching Fund of National Natural Science Foundation of China (81428018); (3) Hunan Provincial Natural Science Foundation of China (14JJ1006, 2016JJ1027); (4) The Project of Innovation-driven Plan of Central South University (2015CXS008, 2016CX023); (5) The Open-End Fund for the Valuable and Precision Instruments of Central South University; (6) The fund of the State Key Laboratory of Solidification Processing at NWPU (SKLSP201605); (7) The fund of the State Key Laboratory for Powder Metallurgy; (8) The Fundamental Research Funds for the Central Universities of Central South University (2017zzts406); and (9) National Postdoctoral Program for Innovative Talents (BX201700291).

Author Contributions: Chenying Shuai and Pei Feng fabricated the scaffolds and carried out the mechanical testing under the supervision of Cijun Shuai, the microstructural characterization of the scaffolds under the supervision of Youwen Yang, Chengde Gao performed the biological testing of the scaffolds under the supervision of Cijun Shuai, the biological characterization of the scaffolds under the supervision of Shuping Peng. All authors discussed the results and implications and approved the final manuscript.

Conflicts of Interest: The authors declare no conflict of interest.

References

1. Goh, Y.F.; Akram, M.; Alshemary, A.; Hussain, R. Antibacterial polylactic acid/chitosan nanofibers decorated with bioactive glass. *Appl. Surf. Sci.* **2016**, *387*, 1–7. [CrossRef]
2. Campana, V.; Milano, G.; Pagano, E.; Barba, M.; Cicione, C.; Salonna, G.; Lattanzi, W.; Logroscino, G. Bone substitutes in orthopaedic surgery: From basic science to clinical practice. *J. Mater. Sci. Mater. Med.* **2014**, *25*, 2445–2461. [CrossRef] [PubMed]
3. Ventola, C.L. The antibiotic resistance crisis: Part 1: Causes and threats. *Pharm. Ther.* **2015**, *40*, 277.

4. Schäberle, T.F.; Hack, I.M. Overcoming the current deadlock in antibiotic research. *Trends Microbiol.* **2014**, *22*, 165–167. [CrossRef] [PubMed]
5. Atalay, H.A.; Canat, L.; Alkan, İ.; Çakir, S.S.; Altunrende, F. Prostate-specific antigen reduction after empiric antibiotic treatment does not rule out biopsy in patients with lower urinary tract symptoms: Prospective, controlled, single-center study. *Prostate Int.* **2017**, *5*, 59–64. [CrossRef] [PubMed]
6. Bisiwe, F.; Rensburg, B.V.; Barrett, C.; Rooyen, C.V.; Vuuren, C.V. Haemodialysis catheter-related bloodstream infections at universitas academic hospital, bloemfontein: Should we change our empiric antibiotics? *S. Afr. J. Infect. Dis.* **2015**, *30*, 29–33. [CrossRef]
7. Cristescu, R.; Visan, A.; Socol, G.; Surdu, A.V.; Oprea, A.E.; Grumezescu, A.M.; Chifiriuc, M.C.; Boehm, R.D.; Yamaleyeva, D.; Taylor, M. Antimicrobial activity of biopolymeric thin films containing flavonoid natural compounds and silver nanoparticles fabricated by maple: A comparative study. *Appl. Surf. Sci.* **2016**, *374*, 290–296. [CrossRef]
8. Nogueira, F.; Granadeiro, L.; Mouro, C.; Gouveia, I.C. Antimicrobial and antioxidant surface modification toward a new silk-fibroin (SG)-L-Cysteine material for skin disease management. *Appl. Surf. Sci.* **2016**, *364*, 552–559. [CrossRef]
9. Lorenzini, C.; Haider, A.; Kang, I.K.; Sangermano, M.; Abbadandalloussi, S.; Mazeran, P.E.; Lalevée, J.; Renard, E.; Langlois, V.; Versace, D.L. Photoinduced development of antibacterial materials derived from isosorbide moiety. *Biomacromolecules* **2015**, *16*, 683–694. [CrossRef] [PubMed]
10. Fan, W.; Wu, D.; Tay, F.R.; Ma, T.; Wu, Y.; Fan, B. Effects of adsorbed and templated nanosilver in mesoporous calcium-silicate nanoparticles on inhibition of bacteria colonization of dentin. *Int. J. Nanomed.* **2014**, *9*, 5217. [CrossRef] [PubMed]
11. Álvarez-Paino, M.; Muñoz-Bonilla, A.; Fernández-García, M. Antimicrobial polymers in the nano-world. *Nanomaterials* **2017**, *7*, 48. [CrossRef] [PubMed]
12. Munoz-Bonilla, A.; Fernandez-Garcia, M. The roadmap of antimicrobial polymeric materials in macromolecular nanotechnology. *Eur. Polym. J.* **2015**, *65*, 46–62. [CrossRef]
13. Yan, Y.; Zhang, X.; Yong, H.; Ding, Q.; Pang, X. Antibacterial and bioactivity of silver substituted hydroxyapatite/TiO_2 nanotube composite coatings on titanium. *Appl. Surf. Sci.* **2014**, *314*, 348–357. [CrossRef]
14. Kubacka, A.; Diez, M.S.; Rojo, D.; Bargiela, R.; Ciordia, S.; Zapico, I.; Albar, J.P.; Barbas, C.; Va, M.D.S.; Fernández-García, M. Understanding the antimicrobial mechanism of TiO_2-based nanocomposite films in a pathogenic bacterium. *Sci. Rep.* **2014**, *4*, 4134. [CrossRef] [PubMed]
15. Muñoz-Bonilla, A.; Cerrada, M.L.; Fernández-García, M.; Kubacka, A.; Ferrer, M.; Fernández-García, M. Biodegradable polycaprolactone–titania nanocomposites: Preparation, characterization and antimicrobial properties. *Int. J. Mol. Sci.* **2013**, *14*, 9249–9266. [CrossRef] [PubMed]
16. Muñoz-Bonilla, A.; Kubacka, A.; Fernández-García, M.; Ferrer, M.; Fernández-García, M.; Cerrada, M.L. Visible and ultraviolet antibacterial behavior in PVDF–TiO_2 nanocomposite films. *Eur. Polym. J.* **2015**, *71*, 412–422. [CrossRef]
17. Bajsić, E.G.; Bulatović Ocelić, V.; Slouf, M.; Šitum, A. Characterization of biodegradable polycaprolactone containing titanium dioxide micro and nanoparticles. *JoMME* **2014**, *8*, 529–533.
18. Hsu, K.C.; Chen, D.H. Highly sensitive, uniform, and reusable surface-enhanced raman scattering substrate with TiO_2 interlayer between ag nanoparticles and reduced graphene oxide. *ACS Appl. Mater. Interfaces* **2015**, *7*, 27571–27579. [CrossRef] [PubMed]
19. Safarpour, M.; Khataee, A.; Vatanpour, V. Preparation of a novel Polyvinylidene Fluoride (PVDF) ultrafiltration membrane modified with reduced Graphene Oxide/Titanium Dioxide (TiO_2) nanocomposite with enhanced hydrophilicity and antifouling properties. *Ind. Eng. Chem. Res.* **2014**, *53*, 13370–13382. [CrossRef]
20. Wang, Y.; Ni, Q.Q.; Zhu, Y.; Natsuki, T. Fabrication of functionally graded nano-TiO_2-reinforced epoxy matrix composites. *Polym. Compos.* **2014**, *35*, 557–563. [CrossRef]
21. Bamedi, M.; Ladiz, M.A.R.; Fakour, S.R.; Bamadi, M. A review of modified titanium nanoparticle applications in dental implantation. *Sci. Int.* **2015**, *4*, 170–174.
22. Shuai, C.; Ping, W.; Zhong, Y.; Pei, F.; Gao, C.; Wei, H.; Zhou, Z.; Li, C.; Shuai, C. Polyetheretherketone/poly(glycolic acid) blend scaffolds with biodegradable properties. *J. Biomater. Sci. Polym. Ed.* **2016**, *27*, 1434–1446. [CrossRef] [PubMed]

23. Gao, C.; Feng, P.; Peng, S.; Shuai, C. Carbon nanotubes, graphene and boron nitride nanotube reinforced bioactive ceramics for bone repair. *Acta Biomater.* **2017**, *61*, 1–20. [CrossRef] [PubMed]
24. Shuai, C.; Feng, P.; Wu, P.; Liu, Y.; Liu, X.; Lai, D.; Gao, C.; Peng, S. A combined nanostructure constructed by graphene and boron nitride nanotubes reinforces ceramic scaffolds. *Chem. Eng. J.* **2017**, *313*, 487–497. [CrossRef]
25. Feng, P.; Peng, S.; Wu, P.; Gao, C.; Huang, W.; Deng, Y.; Xiao, T.; Shuai, C. A nano-sandwich construct built with graphene nanosheets and carbon nanotubes enhances mechanical properties of hydroxyapatite–polyetheretherketone scaffolds. *Int. J. Nanomed.* **2016**, *11*, 3487–3500.
26. Wu, J.Y.; Li, C.W.; Tsai, C.H.; Chou, C.W.; Chen, D.R.; Wang, G.J. Synthesis of antibacterial TiO_2/PLGA composite biofilm. *Nanomedicine* **2013**, *10*, 1097–1107. [CrossRef] [PubMed]
27. González-García, D.M.; Téllez, J.L.; Jiménez-Gallegos, R.; Rodríguez-Lorenzo, L.M. Novel non-cytotoxic, bioactive and biodegradable hybrid materials based on polyurethanes/TiO_2 for biomedical applications. *Mater. Sci. Eng. C Mater. Biol. Appl.* **2017**, *75*, 375–384. [CrossRef] [PubMed]
28. Roether, J.A.; Rai, R.; Wolf, R.; Tallawi, M.; Boccaccini, A.R. Biodegradable poly(glycerol sebacate)/poly(3-hydroxybutyrate)-tionanocomposites: Fabrication and characterisation. *Mater. Sci. Technol.* **2014**, *30*, 574–581. [CrossRef]
29. Naffakh, M.; Díezpascual, A.M.; Marco, C.; Gómez, M.A.; Jiménez, I. Novel melt-processable Poly(ether ether ketone)(PEEK)/inorganic fullerene-like WS_2 nanoparticles for critical applications. *J. Phys. Chem. B* **2010**, *114*, 11444. [CrossRef] [PubMed]
30. Moffat, J.R.; Sefiane, K.; Shanahan, M.E.R. Effect of TiO_2 nano-particles on contact line stck-slip behaviour of volatile drops. *J. Phys. Chem. B* **2009**, *113*, 8860–8866. [CrossRef] [PubMed]
31. And, H.A.B.; Garrett, S.J. TiO_2 nanoparticle arrays prepared using a nanosphere lithography technique. *Nano Lett.* **2002**, *2*, 739–745.
32. Wang, Y.C.; Lin, M.C.; Wang, D.M.; Hsieh, H.J. Fabrication of a novel porous PGA-Chitosan hybrid matrix for tissue engineering. *Biomaterials* **2003**, *24*, 1047–1057. [CrossRef]
33. Kumar, P.; Singh, P.; Pandey, K.N.; Verma, V.; Kumar, V. Poly(ether ether) ketone/poly(ether) imide nanocomposites. *Asian J. Res. Chem.* **2012**, *5*, 703–706.
34. Soares, I.L.; Chimanowsky, J.P.; Luetkmeyer, L.; Da, S.E.; Souza, D.H.; Tavares, M.I. Evaluation of the influence of modified TiO_2 particles on polypropylene composites. *J. Nanosci. Nanotechnol.* **2015**, *15*, 5723–5732. [CrossRef] [PubMed]
35. Zabihi, O. Characterization and thermal decomposition kinetics of Poly(ethylene 2,6-naphthalate) nanocomposites reinforced with TiO_2 nanoparticles. *Polym. Plast. Technol. Eng.* **2012**, *51*, 43–49. [CrossRef]
36. Díezpascual, A.M.; Díezvicente, A.L. Nano-TiO_2 reinforced PEEK/PEI blends as biomaterials for load-bearing implant applications. *ACS Appl. Mater. Interfaces* **2015**, *7*, 5561–5573. [CrossRef] [PubMed]
37. Nakamura, R.; Imanishi, A.; Murakoshi, K.; Nakato, Y. In situ ftir studies of primary intermediates of photocatalytic reactions on nanocrystalline TiO_2 films in contact with aqueous solutions. *J. Am. Chem. Soc.* **2003**, *125*, 7443. [CrossRef] [PubMed]
38. Khaled, S.M.; Charpentier, P.A.; Rizkalla, A.S. Synthesis and characterization of Poly(methyl methacrylate)-based experimental bone cements reinforced with TiO_2–SrO nanotubes. *Acta Biomater.* **2010**, *6*, 3178. [CrossRef] [PubMed]
39. Pascual, A.M.D.; Diez-Vicente, A.L. Effect of TiO_2 nanoparticles on the performance of polyphenylsulfone biomaterial for orthopaedic implants. *J. Phys. Chem. B* **2014**, *2*, 7502–7514.
40. Sharma, P.; Jha, A.B.; Dubey, R.S.; Pessarakli, M. Reactive oxygen species, oxidative damage, and antioxidative defense mechanism in plants under stressful conditions. *J. Bot.* **2012**, *2012*, 217037. [CrossRef]
41. Persat, A.; Nadell, C.D.; Kim, M.K.; Ingremeau, F.; Siryaporn, A.; Drescher, K.; Wingreen, N.S.; Bassler, B.L.; Gitai, Z.; Stone, H.A. The mechanical world of bacteria. *Cell* **2015**, *161*, 988–997. [CrossRef] [PubMed]
42. Sheykhnazari, S.; Tabarsa, T.; Ashori, A.; Ghanbari, A. Bacterial cellulose composites loaded with SiO_2 nanoparticles: Dynamic-mechanical and thermal properties. *Int. J. Biol. Macromol.* **2016**, *93*, 672–677. [CrossRef] [PubMed]
43. Wang, M.; Fan, X.; Thitsartarn, W.; He, C. Rheological and mechanical properties of Epoxy/Clay nanocomposites with enhanced tensile and fracture toughnesses. *Polymer* **2015**, *58*, 43–52. [CrossRef]

44. Pei, F.; Peng, S.; Ping, W.; Gao, C.; Wei, H.; Deng, Y.; Shuai, C. A space network structure constructed by tetraneedlelike ZnO whiskers supporting boron nitride nanosheets to enhance comprehensive properties of poly(L-lacti acid) scaffolds. *Sci. Rep.* **2016**, *6*, 33385.
45. Chou, P.M.; Mariatti, M.; Zulkifli, A.; Sreekantan, S. Evaluation of the flexural properties and bioactivity of bioresorbable PLLA/PBSL/CNT and PLLA/PBSL/TiO_2 nanocomposites. *J. Mater. Sci.* **2012**, *43*, 1374–1381. [CrossRef]
46. Boccaccini, A.R.; Blaker, J.J.; Maquet, V.; Chung, W.; Jérôme, R.; Nazhat, S.N. Poly(D,L-lactide) (PDLLA) foams with TiO_2 nanoparticles and PDLLA/TiO_2-Bioglass® foam composites for tissue engineering scaffolds. *Compos. Part B Eng.* **2006**, *41*, 3999–4008. [CrossRef]
47. Avolio, R.; D'Albore, M.; Guarino, V.; Gentile, G.; Cocca, M.C.; Zeppetelli, S.; Errico, M.E.; Avella, M.; Ambrosio, L. Pure titanium particle loaded nanocomposites: Study on the polymer/filler interface and hmsc biocompatibility. *J. Mater. Sci. Mater. Med.* **2016**, *27*, 153. [CrossRef] [PubMed]
48. Signoretto, M.; Ghedini, E.; Nichele, V.; Pinna, F.; Casotti, D.; Cruciani, G.; Aina, V.; Martra, G.; Cerrato, G. Formulation of innovative hybrid Chitosan/TiO_2- and Chitosan/SiO_2-based drug-delivery systems. In *Nanoarchitectonics for Smart Delivery and Drug Targeting*; William Andrew Inc.: New York, NY, USA, 2016; pp. 201–226.
49. Gao, C.; Peng, S.; Feng, P.; Shuai, C. Bone biomaterials and interactions with stem cells. *Bone Res.* **2017**, *5*, 17059. [CrossRef] [PubMed]

© 2018 by the authors. Licensee MDPI, Basel, Switzerland. This article is an open access article distributed under the terms and conditions of the Creative Commons Attribution (CC BY) license (http://creativecommons.org/licenses/by/4.0/).